

Simulation of a Variety of Wings Using a Reynolds Stress Model

K. B. Thompson* and H. A. Hassan†

North Carolina State University, Raleigh, North Carolina 27695-7910

DOI: 10.2514/1.C033046

The Wilcox 2006 stress- ω model, a Reynolds stress model, implemented in both the NASA Langley codes FUN3D and CFL3D, has been used to study a number of 2-D and 3-D cases. This study continues the assessments of the stress- ω model by simulating the flow over two wings: the DPW-W1 and the DLR-F11 wings. Using FUN3D, which uses unstructured grids, and CFL3D, which uses structured grids, the results were compared to solvers employing one- and two-equation turbulence models and experimental data. In general, in situations where experimental data is available, the stress- ω model performs as well or better than one- and two-equation models.

Nomenclature

AR	=	wing aspect ratio
b	=	wing full span
C_p	=	pressure coefficient
C_{ref}	=	wing mean aerodynamic chord
M	=	Mach number
Re	=	Reynolds number
S_{ref}	=	wing reference area
T_{ref}	=	reference temperature
X_{ref}	=	x -direction pitching moment reference
Y_{ref}	=	y -direction pitching moment reference
Z_{ref}	=	z -direction pitching moment reference
α	=	angle of attack
χ	=	U-MUSCL scheme coefficient

I. Introduction

SIMULATING flows over wing geometries has been studied extensively. Researchers have applied one- and two-equation turbulence models to predict many flow features, but these results may not always be satisfactory. Turbulent Reynolds stress models (RSM) offer a variety of appealing features: not relying on the linear relationship between Reynolds stress and strain rate tensor, they include the effects of curvature and rotation and resolve the normal stress anisotropy near walls. The purpose of this study is to determine whether a Reynolds stress model can provide more accurate results in simulating flow over complex wing shapes using different grids and flow solvers. In an earlier investigation [1], the Wilcox 2006 stress- ω model [2] was used to study a variety of two-dimensional flows and the ONERA M6 and NASA Trapezoidal wing, using CFL3D [3].

In this earlier study [1], the stress- ω model was shown to provide results consistent with one- and two-equation turbulence models for both transonic and high-lift wing cases. A primary motivator for using a RSM was to determine whether it could better predict flow separation than a simpler one- or two-equation turbulence model. It was found that, for the ONERA M6 wing, the Spalart–Allmaras (SA) model, the shear stress transport (SST) model, and Wilcox 2006 stress- ω RSM gave similar results, and for the NASA Trapezoidal wing, the RSM and SST model performed comparably. All of these

cases were run using structured grids on the structured grid code, CFL3D, and a primary interest for this current research is to determine whether the RSM performs well using an unstructured grid code.

For the work in this paper, the Wilcox 2006 stress- ω model [2] is used to simulate other wings. The model is a second-moment RSM consisting of five mean-flow conservation equations, six stress equations, and one length scale equation. The stress- ω model is largely distinguished from other second-moment RSMs by its length scale equation. Where other models, such as the Launder–Reece–Rodi [4] model, are based upon the ε -equation, the stress- ω length scale equation is based upon the ω -equation, and thus avoids the problems near the wall associated with the ε -equation. This RSM was recently implemented into the NASA Langley FUN3D [5] code and validated with extensive comparison to test cases available on the NASA Langley Turbulence Modeling Resource website.[‡]

This research focuses on two wings, the DPW-W1 wing from the 3rd AIAA Drag Prediction Workshop [6] and the DLR-F11 wing from the 2nd High Lift Prediction Workshop [7]. These two wings represent a cruise-type configuration and a high-lift configuration representative of realistic aircraft configurations. The 3rd AIAA Drag Prediction Workshop conducted an extensive study on the DPW-W1 wing, with flow simulation done by a variety of flow solvers for structured and unstructured grids. A statistical framework was used to validate the results, and all results made available. These results included pressure and skin friction coefficient predictions at various span-wise positions. The 2nd High Lift Prediction Workshop also conducted a similar study, and also collected experimental data from two wind tunnel facilities.

II. Wing Geometries

The DPW-W1 is a simple wing-alone model, designed to be representative of a supercritical section found on most transport aircraft, and it is shown in Fig. 1. The key features of this wing are given as follows: $S_{ref} = 290322 \text{ mm}^2$, $C_{ref} = 197.556 \text{ mm}$, $b/2 = 762 \text{ mm}$, $AR = 8.0$, $X_{ref} = 154.245 \text{ mm}$, $Y_{ref} = 0.0 \text{ mm}$, $Z_{ref} = 0.0 \text{ mm}$.

All moment reference coordinates are based on an origin at the wing root leading edge. No flap or aircraft fuselage is attached to this wing, and simulation was conducted as though in a free-air environment.

The DLR-F11 model represents a three element high lift wing configuration in landing configuration and an attached body pod, shown in Figs. 2 and 3. The model included slat and flap track fairings that will hence be referred to as “brackets”. The key features of this wing-body configuration are given as follows: $S_{ref} = 419130 \text{ mm}^2$, $C_{ref} = 347.09 \text{ mm}$, $b/2 = 1400 \text{ mm}$, $AR = 9.353$, $X_{ref} = 1428 \text{ mm}$, $Y_{ref} = 0.0 \text{ mm}$, $Z_{ref} = -41.61 \text{ mm}$.

Presented as Paper 2014-2192 at the AIAA Aviation and Aeronautics Forum and Exposition 2014, Atlanta, GA, 16–20 June 2014; received 26 June 2014; revision received 31 October 2014; accepted for publication 18 December 2014; published online 26 February 2015. Copyright © 2014 by the American Institute of Aeronautics and Astronautics, Inc. All rights reserved. Copies of this paper may be made for personal or internal use, on condition that the copier pay the \$10.00 per-copy fee to the Copyright Clearance Center, Inc., 222 Rosewood Drive, Danvers, MA 01923; include the code 1533-3868/15 and \$10.00 in correspondence with the CCC.

*Graduate Research Assistant, Mechanical and Aerospace Engineering, Student Member AIAA.

†Professor, Mechanical and Aerospace Engineering, Fellow AIAA.

[‡]<http://turbmodels.larc.nasa.gov/>.

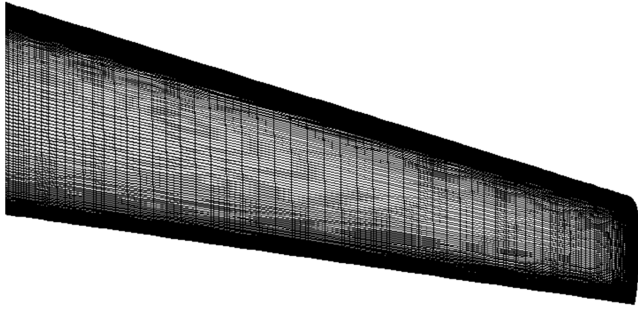


Fig. 1 DPW-W1 Surface Mesh.

The moment reference coordinates are based on an origin at the nose of the body pod. The 2nd AIAA High Lift Prediction Workshop included data taken from two wind tunnels. A lower Reynolds number flight condition of 1.35 million was conducted in the low-speed wind tunnel Airbus-Deutschland (B-LSWT), and a high Reynolds number flight condition of 15.1 million was conducted at the European Transonic Windtunnel (ETW) [7]. Both facilities collected a large amount of pressure, velocity, and force/moment data, as well as oil flow visualizations.

III. Test Conditions and Grid Systems

The 3rd AIAA Drag Prediction Workshop focused on solver-to-solver comparison for transonic flow. The DPW-W1 test conditions were $Re = 5.0 \times 10^6$ (based on DPW-W1 C_{ref}), $M = 0.76$, $T_{ref} = 322$ K, $\alpha = 0.5$ deg. The grid used was an structured mesh generated by the Ed Tinoco of Boeing, consisting of 14.7 million grid points. The grid was also converted to an unstructured hexahedral mesh so that this case could be run using FUN3D. This grid was

previously used by various in the workshop, with the Spalart-Allmaras turbulence model [8].

The 2nd AIAA High Lift Prediction Workshop focused on the lower-speed, landing stage of flight. The DLR-F11 high Reynolds number test conditions were $Re = 15.1 \times 10^6$ (based on DLR-F11 C_{ref}), $M = 0.175$, $T_{ref} = 114.0$ K, $\alpha = 7$ deg. The lower Reynolds number test conditions were identical to the previous test conditions, except for $Re = 1.35 \times 10^6$ (also based on DLR-F11 C_{ref}), $T_{ref} = 298.6$ K, and $\alpha = 7, 16, 18.5$ deg. For FUN3D, the grids used were the mixed element “D” medium grids, generated by Cessna and the University of Wyoming. The grids were created by merging the pure tetrahedral “D” medium grid with prisms in the boundary layer. For the high Reynolds number case, the grid did not include brackets, and consisted of 30.8 million nodes. For the low Reynolds number case, the grid included brackets and consisted of 41.5 million grid points. Both were previously used by FUN3D in the workshop, with the Spalart-Allmaras turbulence model. For CFL3D, the grid used was the structured “A” grid, generated by Boeing, and was used only for the high Reynolds number case in the workshop. The grid did not include brackets, consisted of 34.3 million points, and was previously used in CFL3D with the Spalart-Allmaras turbulence model.

IV. Computational Approach

FUN3D is an unstructured, nodal-based, parallel 3-D compressible finite-volume grid code, which is capable of using mixed element meshes. An upwind Roe [9] scheme is used in this study, and second order accuracy is obtained by updating face values using a U-MUSCL scheme [10] with the χ set as 0.5 for both cases. All gradients at mesh vertices are computed using a least-squares technique. Time-stepping is done based on a backwards Euler time differencing scheme. The linear system of equations is solved with a line implicit procedure that is used as a preconditioner for generalized conjugate residual [11], which helps to stabilize and accelerate convergence. No limiter was used for the DLR-F11 case, as it was not needed, and a minmod limiter was used for the DPW-W1 case. The



Fig. 2 DLR-F11 model in the B-LWST wind tunnel.

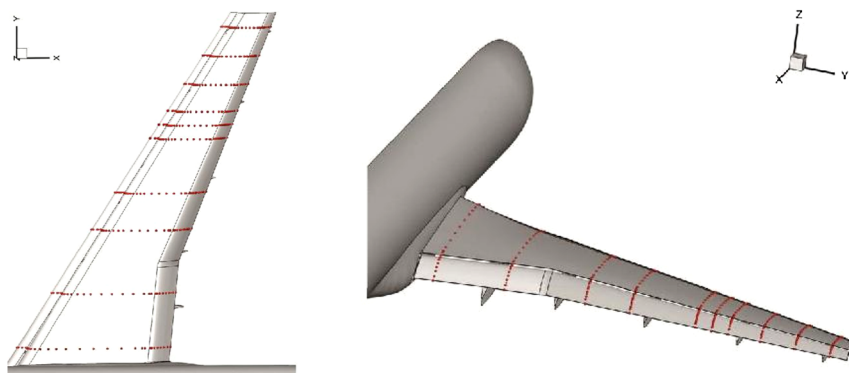


Fig. 3 DLR-F11 pressure tap locations.

turbulence equations are solved separately from the mean flow equations.

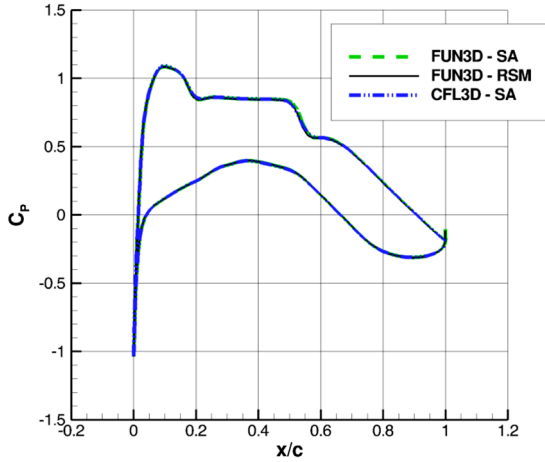
CFL3D is a structured, cell-centered, parallel 3-D compressible finite-volume grid code. An upwind Roe flux difference-splitting method [9] is used in this study, with third-order spatial differencing used to compute the convective terms, and second-order central differencing used to compute the viscous terms. No limiter was used for the DLR-F11 case, as it was not needed, and a minmod limiter was used for the DPW-W1 case. The turbulence equations are solved separately from the mean flow equations, using a first-order

advection scheme, and time advancement is based on a backward Euler scheme, with an implicit approximate factorization method.

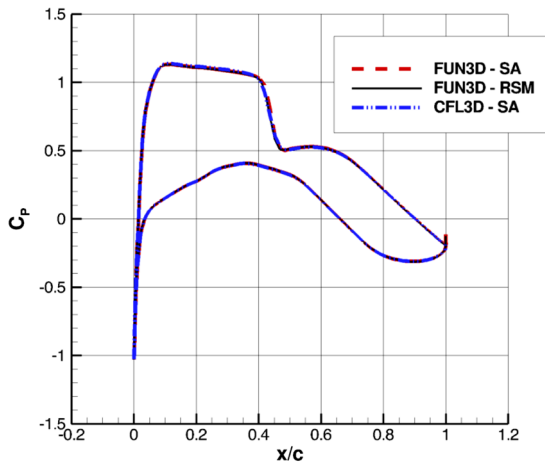
V. Results

A. DPW-W1

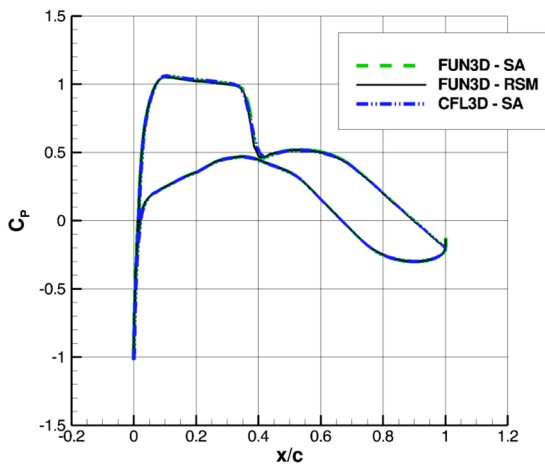
Figure 4 shows the comparison of pressure coefficients at various span positions along the wing. Since no experimental data was



a) DPW-W1 at $y = 120$ mm

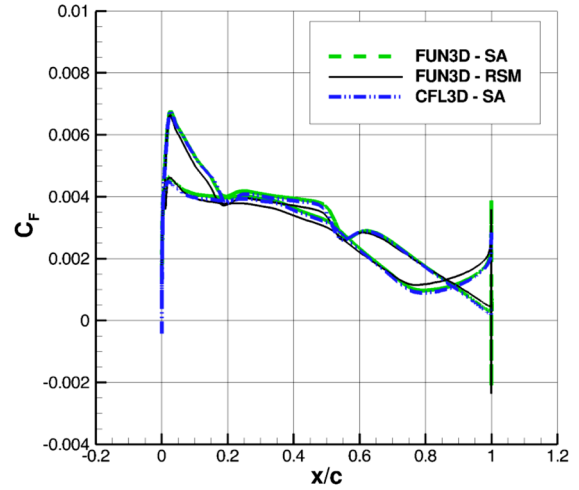


b) DPW-W1 at $y = 320$ mm

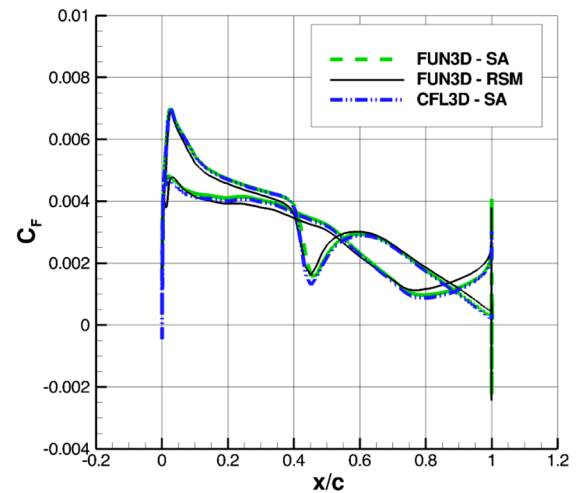


c) DPW-W1 at $y = 620$ mm

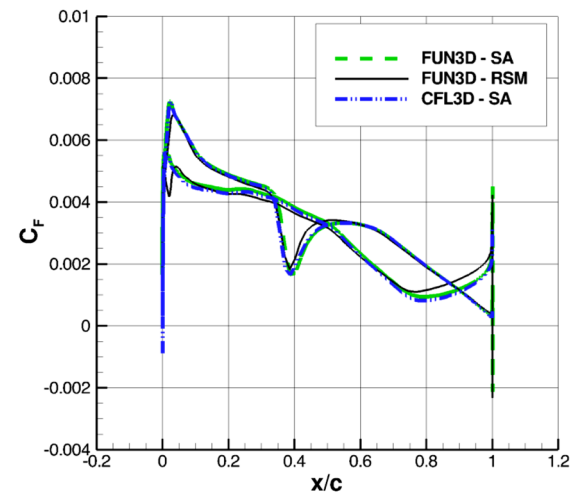
Fig. 4 Pressure coefficients at $\alpha = 0.5$ deg.



a) DPW-W1 at $y = 120$ mm



b) DPW-W1 at $y = 320$ mm



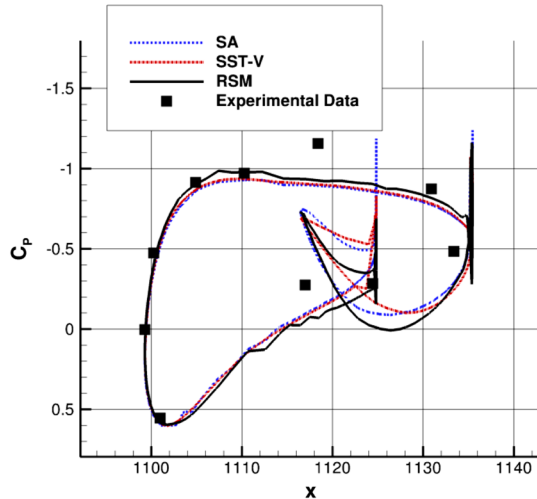
c) DPW-W1 at $y = 620$ mm

Fig. 5 Skin friction coefficients at $\alpha = 0.5$ deg.

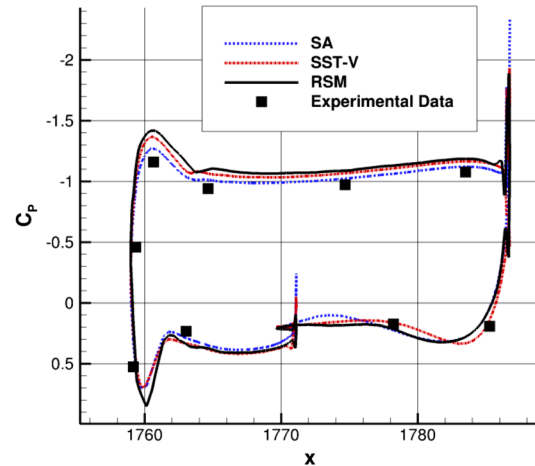
collected for this geometry, a solver-to-solver comparison is made to demonstrate consistency. The comparison is made between FUN3D and CFL3D, both running on the very fine hexahedral grid generated by Ed Tinoco for the 3rd AIAA Drag Prediction Workshop. Figure 4 shows that there is nearly exact agreement in the pressure coefficient between these solvers at all spanwise locations for the SA turbulence

model, and that the RSM run using FUN3D also agrees with the pressure distribution. This consistency between the results of different codes running on the same grid helps validate the implementation of the RSM in FUN3D.

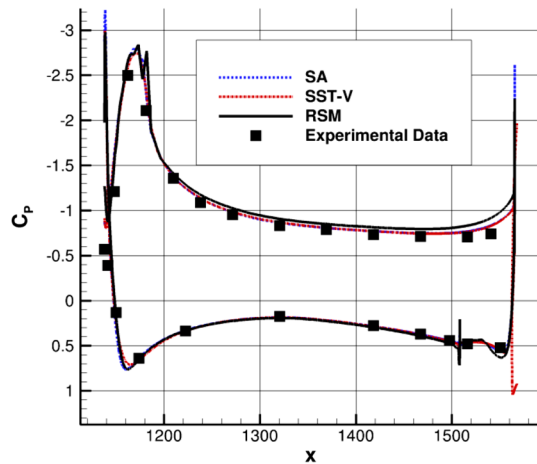
The skin friction coefficient comparison is shown in Fig. 5. The RSM results are similar to SA model results from the FUN3D and



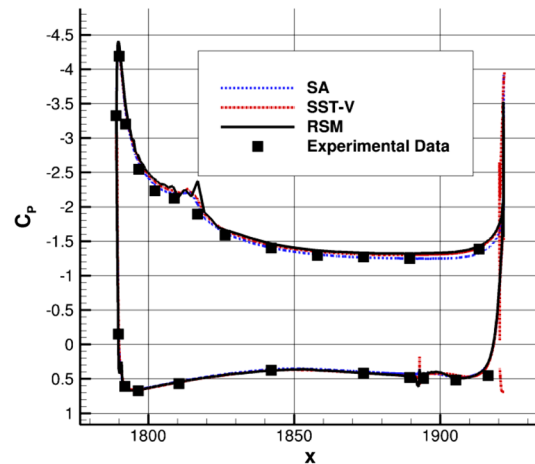
a) Slat at $2y/B = 0.15$, no brackets



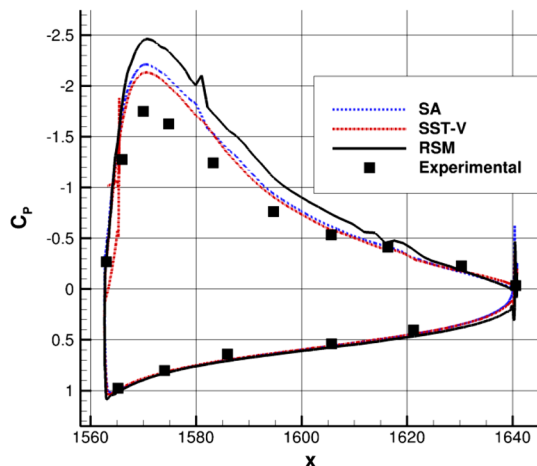
b) Slat at $2y/B = 0.89$, no brackets



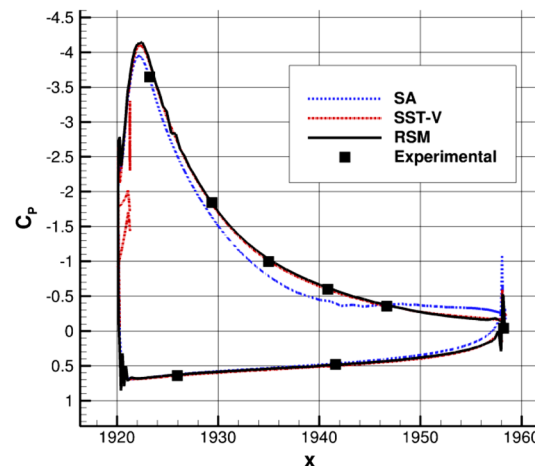
c) Main wing at $2y/B = 0.15$, no brackets



d) Main wing at $2y/B = 0.89$, no brackets



e) Flap at $2y/B = 0.15$, no brackets



f) Flap at $2y/B = 0.89$

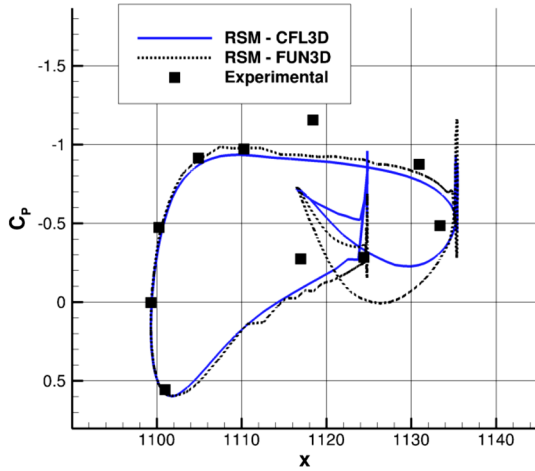
Fig. 6 Surface pressure coefficients for two span locations at $\alpha = 7$ deg, $Re = 1.5 \times 10^6$.

CFL3D, and while there are differences between the FUN3D and CFL3D SA model results, these differences are of a much lower order than the RSM differences. There is clearly shock-boundary layer interaction captured by all the models, and the RSM shows very strong agreement with the SA model results except for the aft portion of the wing, where the RSM predicts higher skin friction coefficients. This can be explained by the fact that the RSM is less dissipative the

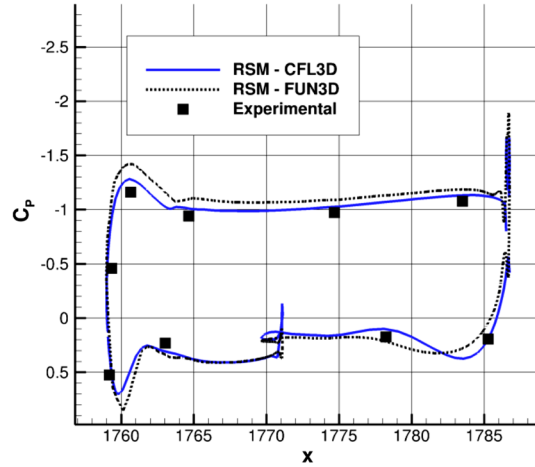
SA model, and therefore results in higher skin friction. Again, the consistency in the results helps validate the RSM implementation in FUN3D.

B. DLR-F11

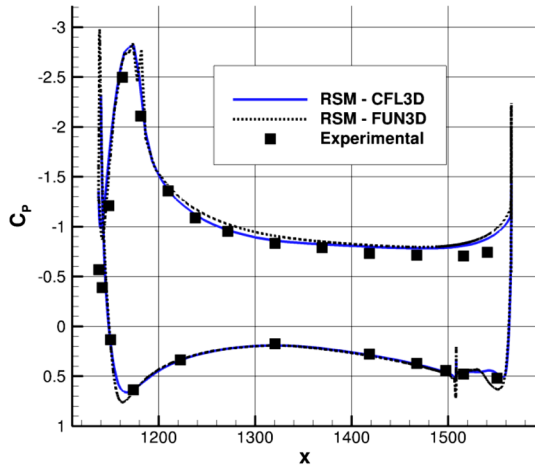
The surface pressure coefficients for the high Re case are shown in Fig. 6, comparing the FUN3D simulations using the Spalart



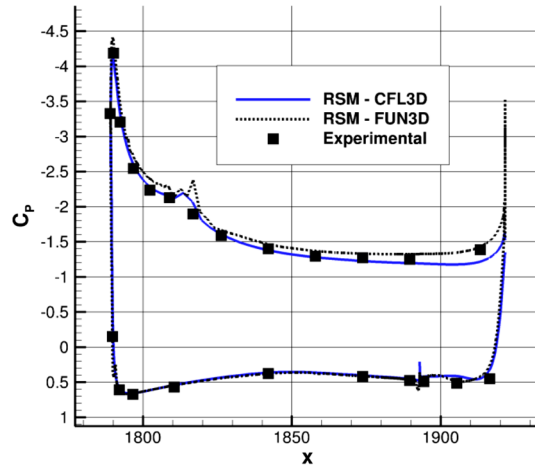
a) Slat at $2y/B = 0.15$, no brackets



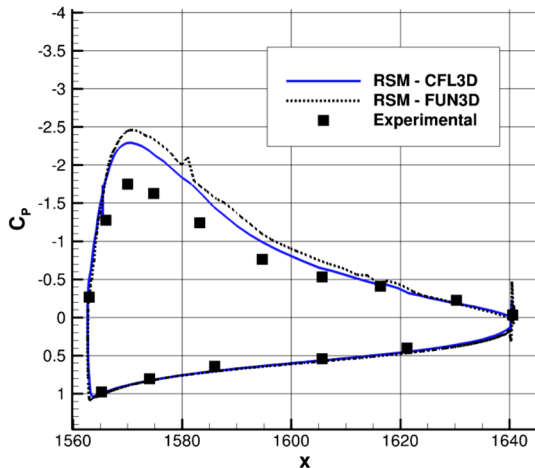
b) Slat at $2y/B = 0.89$, no brackets



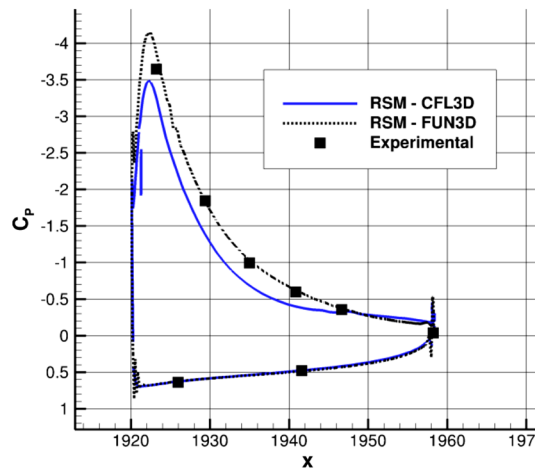
c) Main wing at $2y/B = 0.15$, no brackets



d) Main wing at $2y/B = 0.89$, no brackets



e) Flap at $2y/B = 0.15$, no brackets



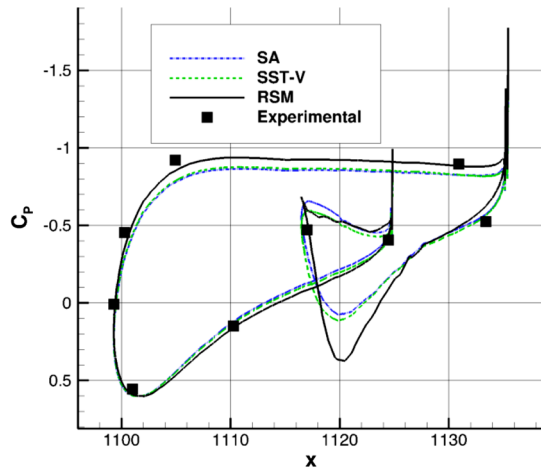
f) Flap at $2y/B = 0.89$

Fig. 7 Surface pressure coefficients for two span locations at $\alpha = 7$ deg, $Re = 1.5 \times 10^6$.

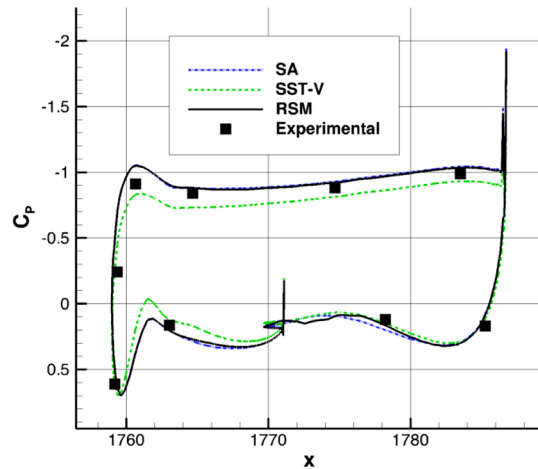
Allmaras, SST-V (SST [12] with a vorticity source term) and stress- ω turbulence models, as well as experimental data collected at the ETW facility. All calculations of the DLR-F11 case were computed assuming fully turbulent flow. The RSM performs as well as the two-equation SST-V turbulence model in almost all cases, and outperforms the SA model in the out-board flap in Fig. 6f. However, all models show a lack of agreement with the experiment in the lower

region of the slat, where separation takes place, and all models underpredicted C_p on the upper surface of the flap at $2y/b = 0.15$, with the stress- ω model showing the highest departure from the experiment.

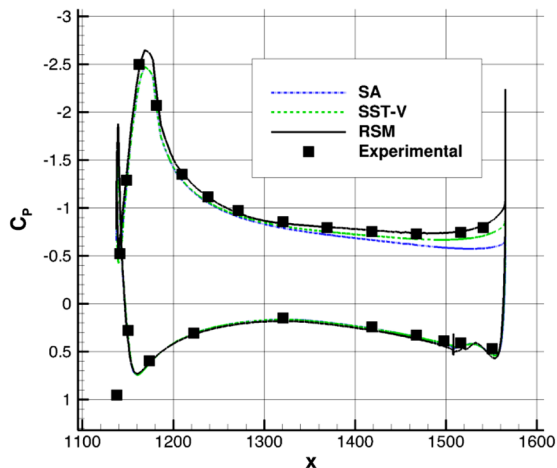
In order to check consistency between FUN3D and CFL3D, both were used with the RSM for the high Re case at 7 deg angle of attack. Figure 7 shows differences in the surface pressure



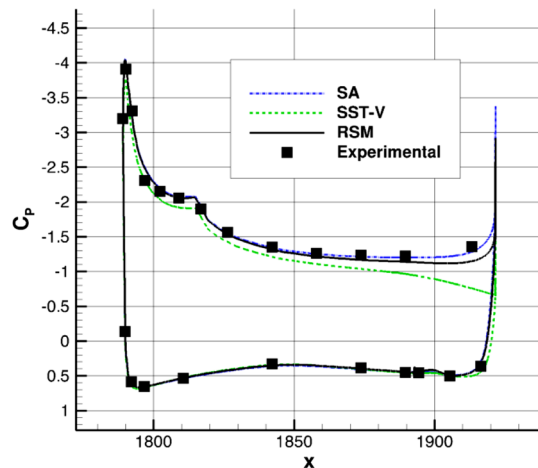
a) Slat at $2y/B = 0.15$, w/brackets



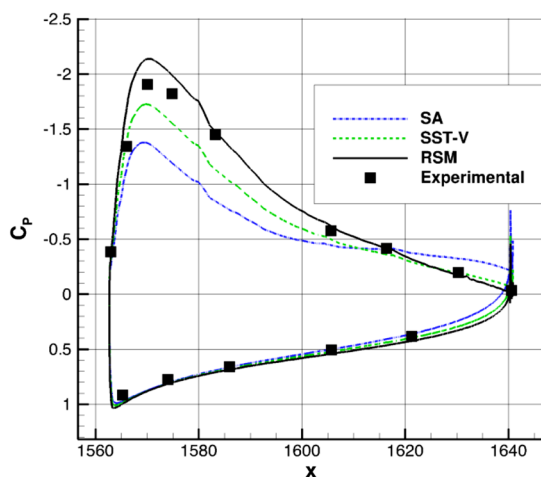
b) Slat at $2y/B = 0.89$, w/brackets



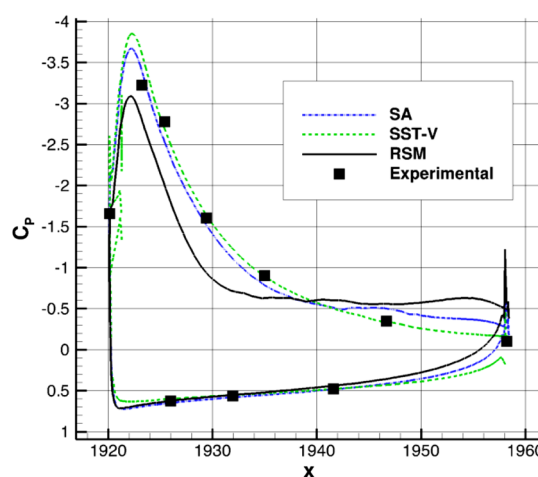
c) Main wing at $2y/B = 0.15$, w/brackets



d) Main wing at $2y/B = 0.89$, w/brackets



e) Flap at $2y/B = 0.15$, w/brackets

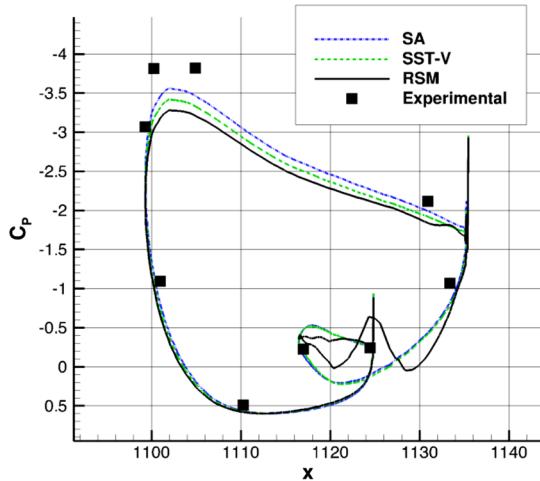


f) Flap at $2y/B = 0.89$, w/brackets

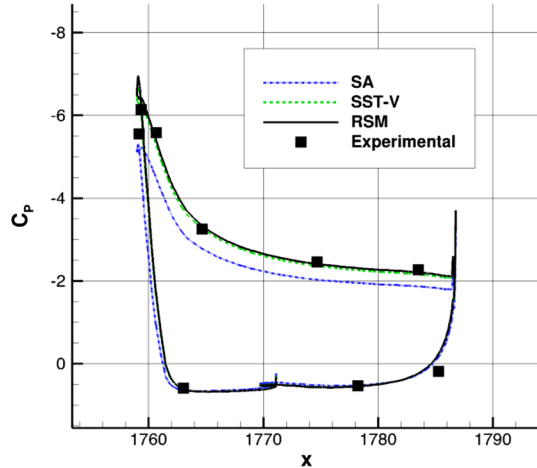
Fig. 8 Surface pressure coefficients for two span locations at $\alpha = 7$ deg, $Re = 1.35 \times 10^6$.

coefficients, with CFL3D performing better at most locations, except the outboard flap region. These differences can be attributed to differences between the grids used by both solvers and to differences in how the algorithm is employed by both codes. CFL3D was previously used to simulate numerous 2-D and 3-D flows, and it was shown to perform well in comparison to one- and two-equation turbulence models [1]. Given the previous near-exact consistency

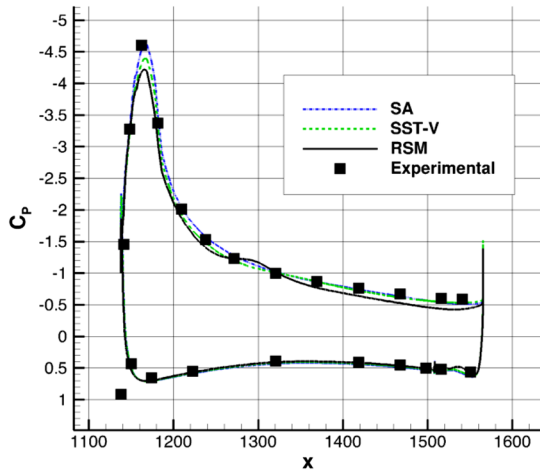
between CFL3D and FUN3D pressure distribution predictions for the DPW-W1 case, it is likely that the discrepancies between the codes are due to differences between the structured “A” grid, used by CFL3D, and the mixed element, unstructured “D” grid, used by FUN3D. This indicates that the solution is sensitive to the mesh, and that computation should be done on a consistent grid to fully define the cause and scope of the differences between the codes’ predictions.



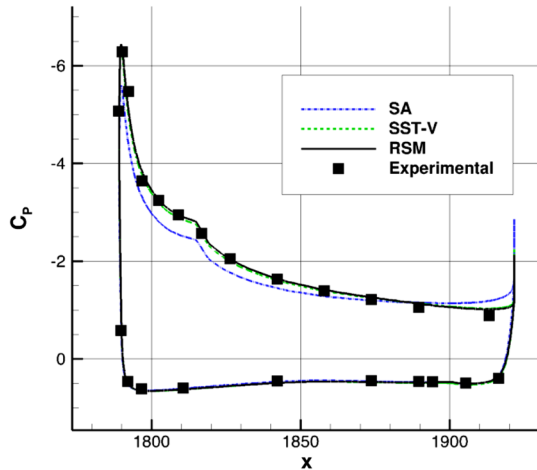
a) Slat at $2y/B = 0.15$, w/brackets



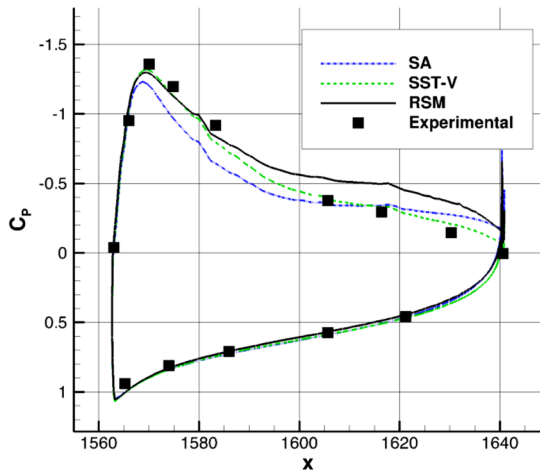
b) Slat at $2y/B = 0.89$, w/brackets



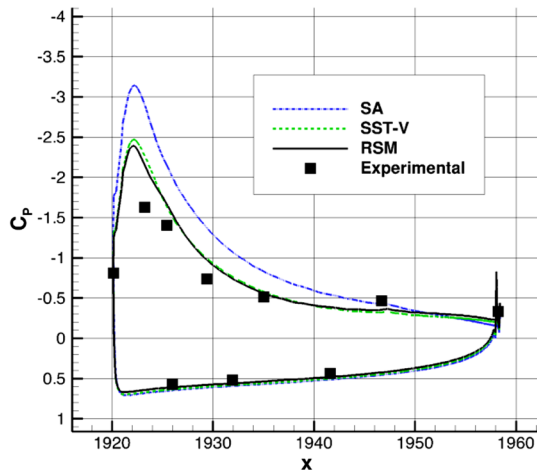
c) Main wing at $2y/B = 0.15$, w/brackets



d) Main wing at $2y/B = 0.89$, w/brackets



e) Flap at $2y/B = 0.15$, w/brackets



f) Flap at $2y/B = 0.89$, w/brackets

Fig. 9 Surface pressure coefficients at for two span locations at $\alpha = 18, 5$ deg, $Re = 1.35 \times 10^6$.

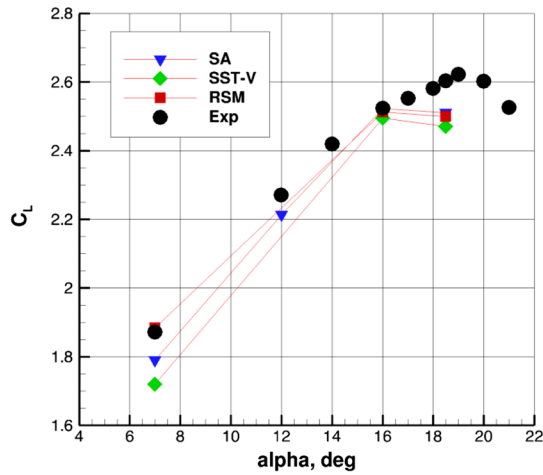
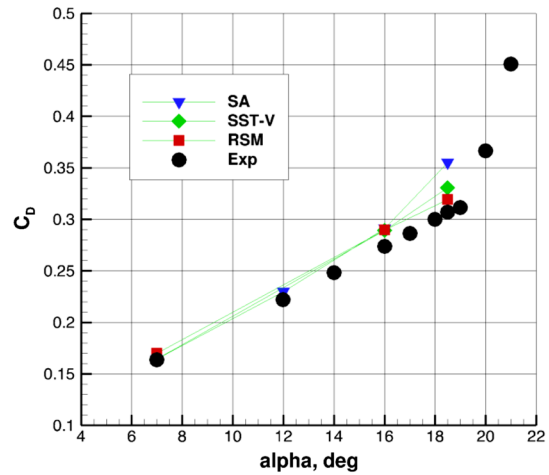
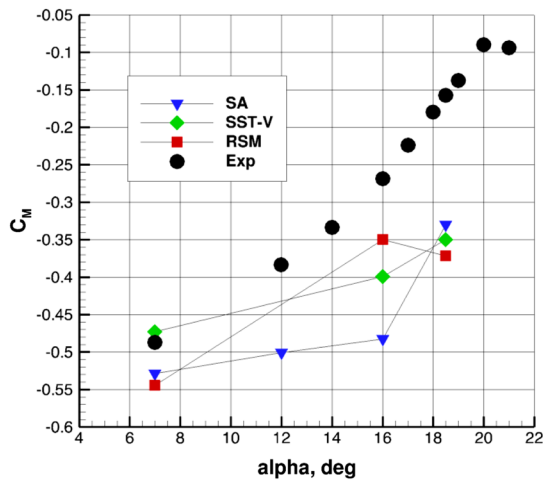
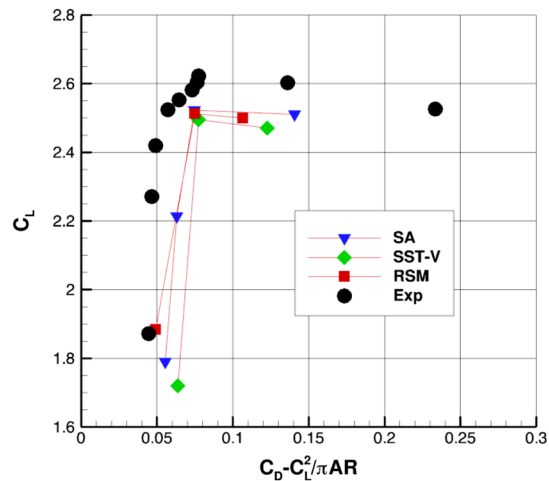
a) C_L , $Re = 1.35 \times 10^6$ b) C_D , $Re = 1.35 \times 10^6$ c) C_M , $Re = 1.35 \times 10^6$ d) Drag polar, $Re = 1.35 \times 10^6$

Fig. 10 Forces and pitching moments (with brackets).

Unfortunately, FUN3D was never able to be successfully run on the “A” grid, due to the mesh topology near the wall, which led to numerical instabilities in the unstructured code that did not arise for CFL3D.

A comparison is made between the FUN3D solutions employing the SA and SST-V turbulence models, the RSM, and the experimental surface pressure data, shown in Figs. 8 and 9. As stated before, all computations were run fully turbulent, and given the low Reynolds number for this case, transition is expected to affect the results; therefore, the comparisons made between turbulence models for this case are intended to show a relative improvement in accuracy between two models neglecting transition effect, and not necessarily a uniform improvement in model performance. The RSM predicts surface pressures comparable to the SST-V model in most cases, and both of these match the experimental data more closely than the SA model in most cases. Figures 8e, 9e, and 9f show that the RSM performs especially well on the flap, particularly where the SA turbulence model significantly over-predicts the pressure at the higher angle of attack. Moreover, stress- ω shows better agreement with experiment on the slat. This is significant, because most codes in the 2nd AIAA High Lift Prediction Workshop had the greatest error in this region [7].

For the low Re case, Fig. 10 shows that the RSM does a good job predicting lift and drag up to 16 deg angle of attack, while the SST-V and SA model underpredict the lift at 7 and 16 deg angle of attack. All of the models failed to make accurate predictions at the higher angle of attack, with the RSM predictions better matching the measured drag coefficient, and the SA and SST-V models more closely

matching the pitching moment coefficient. This discrepancy at high angles of attack warrants further investigation into the mesh sensitivity and the effect of transition may better explain the results. The improvement in drag predictions by the RSM at the high angle of

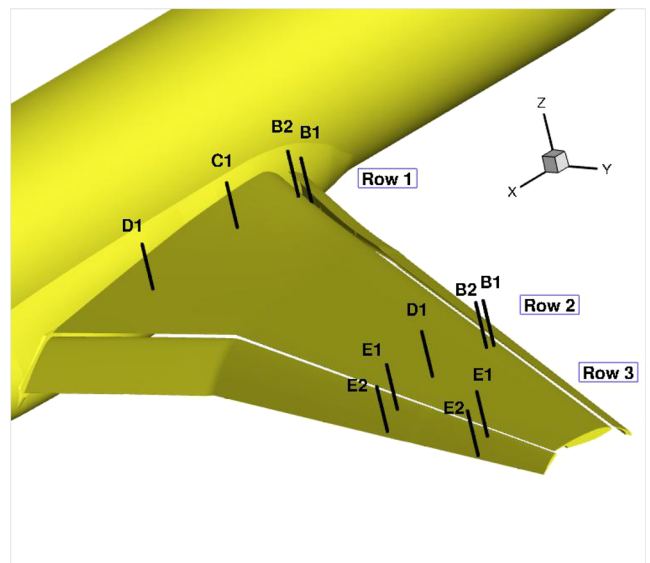


Fig. 11 Velocity profile locations.

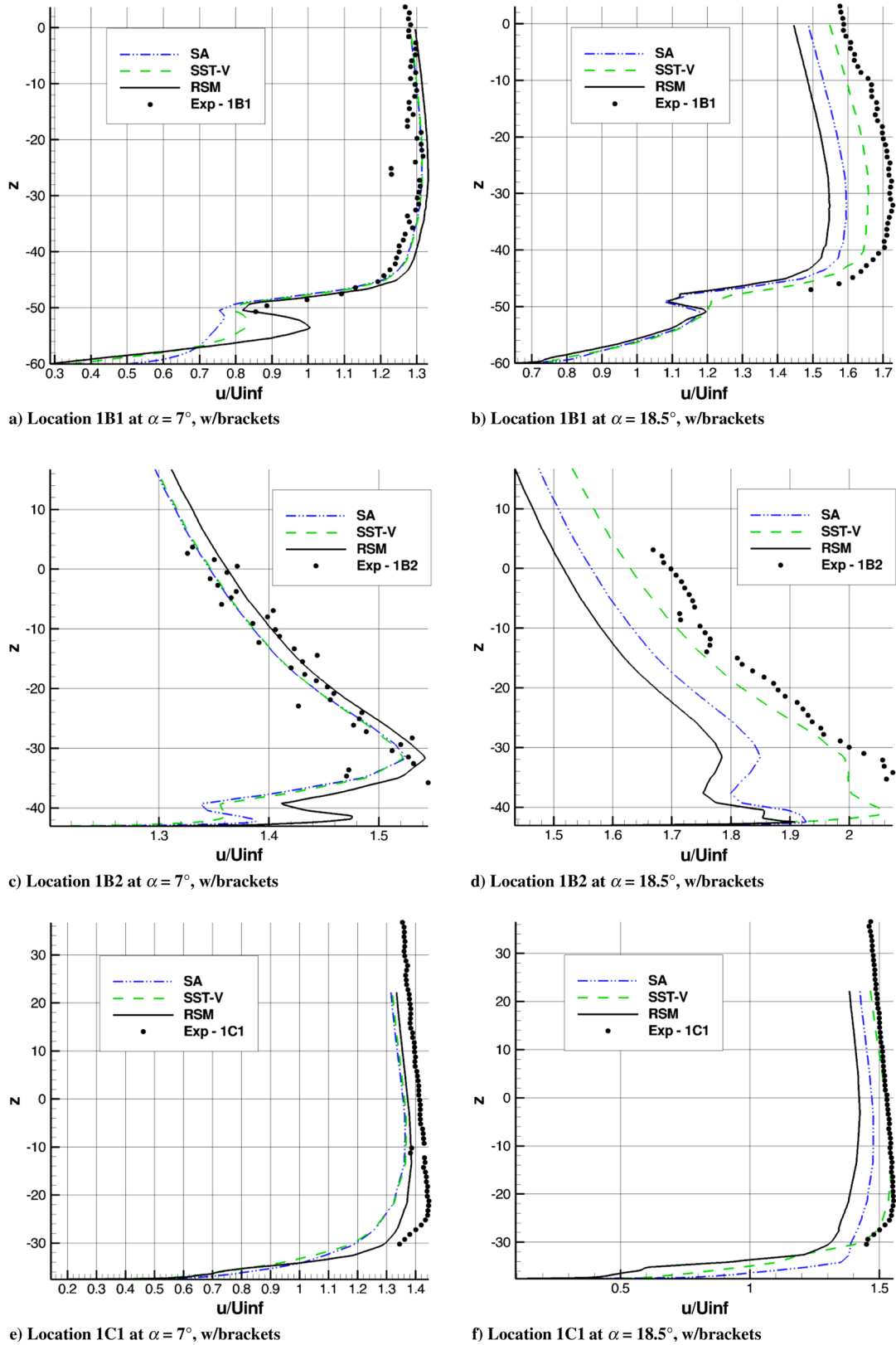


Fig. 12 Velocity profiles (part 1) at $Re = 1.35 \times 10^6$.

attack is suspected to be due to the effect of streamline curvature and normal stress, both of which are both included in the RSM, but not in the SA or SST-V turbulence models. It should also be noted that the wind tunnel wall the half-model affects the DLR-F11 experimental results where the half-model is installed [13]. This affects the inboard section of the wing, and is a cause of over-predicted drag in the tunnel.

Figure 11 shows a sketch of the locations where velocities were measured using particle image velocimetry (PIV) in the B-LSWT wind tunnel. Figures 12–14 show comparisons of representative velocity profiles between FUN3D running the SA model and RSM, and SST-V model. All models do poorly in comparison to the experimental measurement. This was true for many unstructured flow solvers in the 2nd High Lift Prediction Workshop, and none the

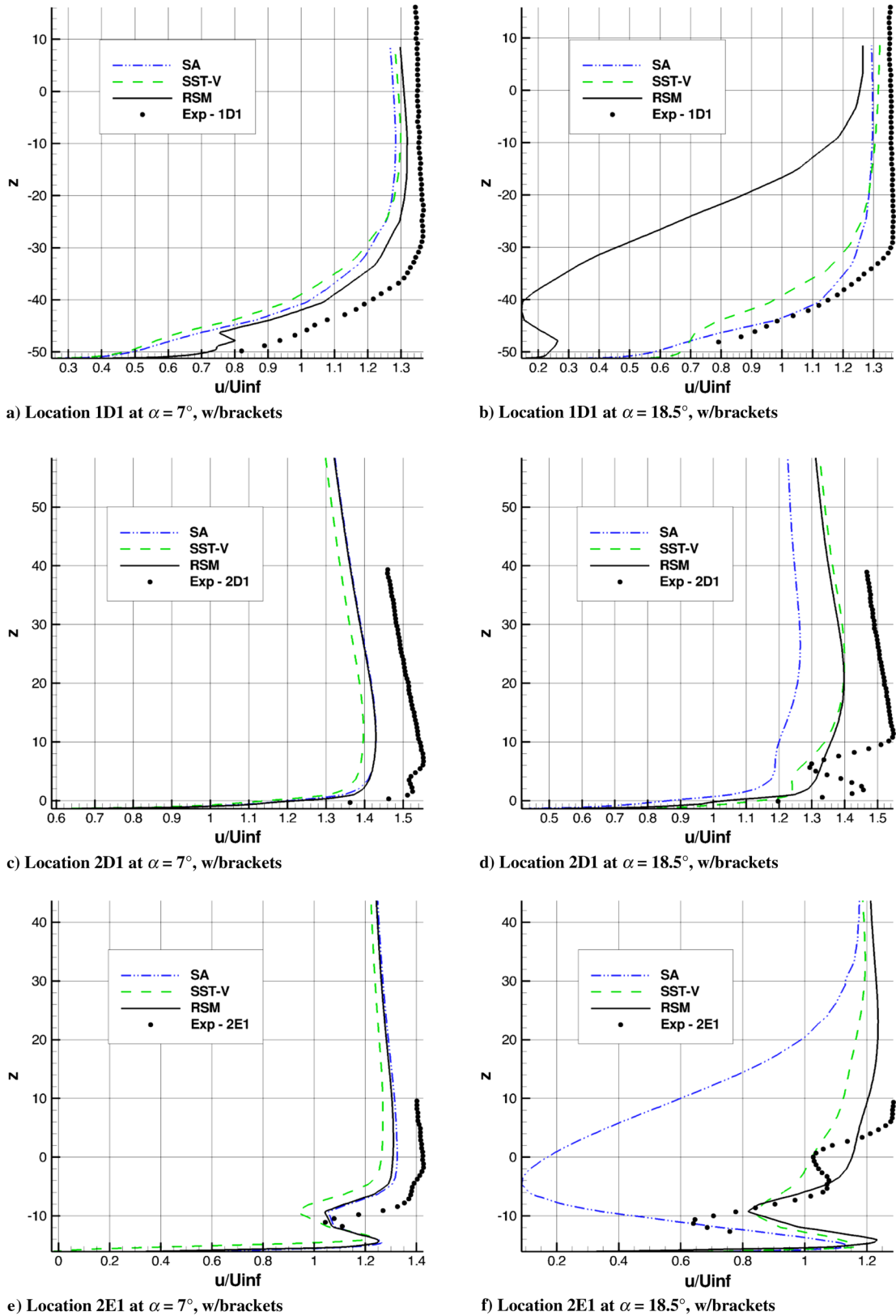


Fig. 13 Velocity profiles (part 2) at $Re = 1.35 \times 10^6$.

participants accurately predicted the wake regions due to poor grid resolution in these areas. There is very little difference overall in the predictions of any of the models where the effects of the wake are very small. Overall, all of the models usually underpredicted the velocity at the lower angle of the attack of 7 deg. The RSM does perform better than the SA and SST-V turbulence models at the outboard stations,

especially in the presence of a large wake, whereas the SST-V turbulence model better matches the experimental data at the inboard stations than the SA model and RSM. In addition to poor grid resolution, these discrepancies could also be attributed to neglecting transition. Since this is a low-Reynolds number test condition, transition likely has an effect on many aspects of this simulation, but

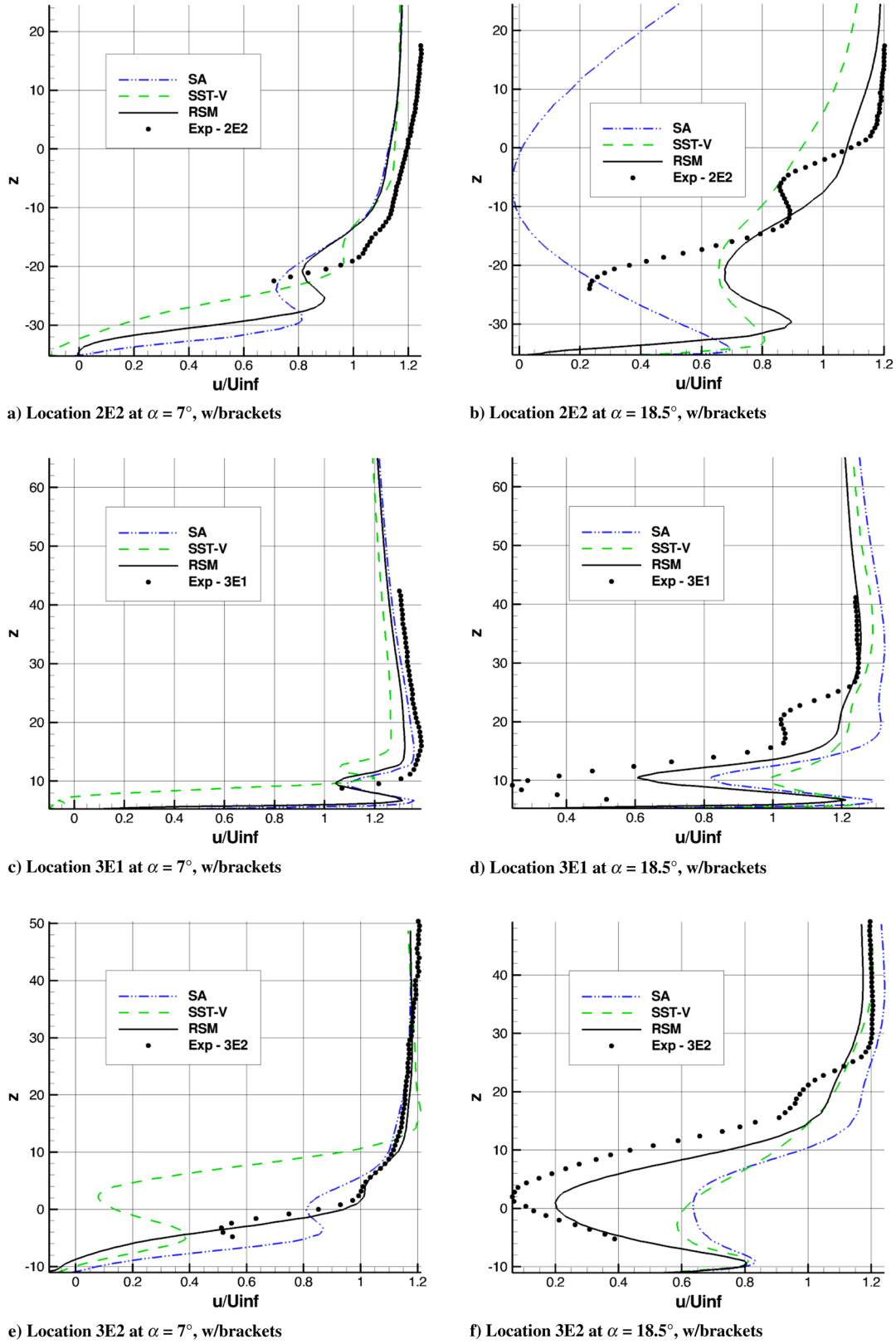
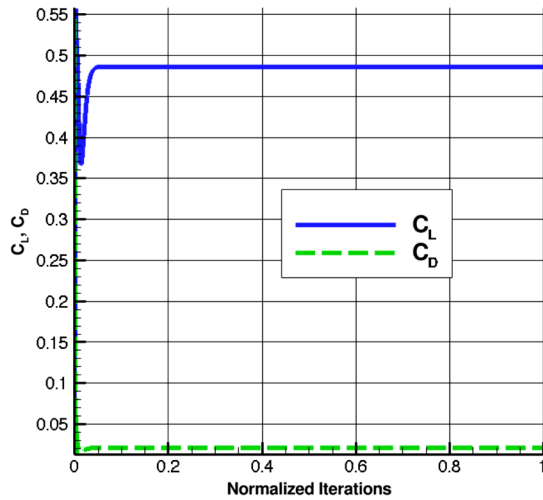


Fig. 14 Velocity profiles (part 3) at $Re = 1.35 \times 10^6$.

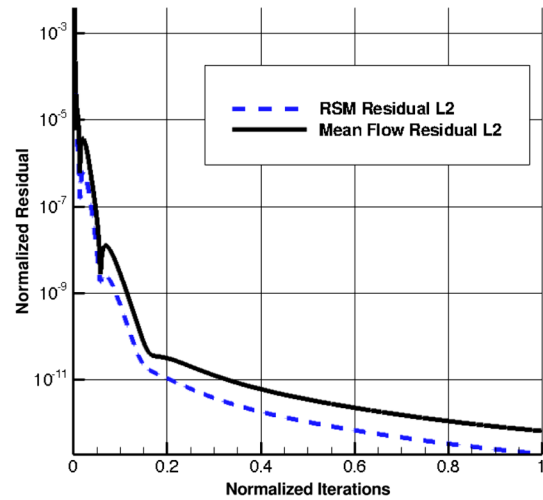
as there currently is no capability in either FUN3D or CFL3D for simulating transition using the RSM, a fully turbulent simulation was conducted in this study.

Convergence of the RSM was shown to differ between the two geometries. Figures 15 and 16 show the convergence of normalized residuals and lift and drag coefficients for FUN3D. In both figures,

the mean flow and turbulence equation normalized residuals were computed as l^2 -norms to best represent the total residual. Figure 15 shows the mean flow and turbulence equation residuals converged to nearly machine zero for double precision, and the lift and drag coefficients were both steady at convergence. Figure 16 shows that mean flow and turbulence equation residuals converged to the order

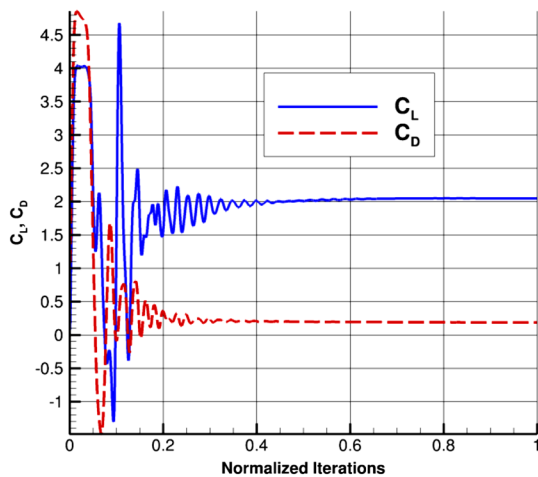


a) DPW-W1 lift and drag coefficients

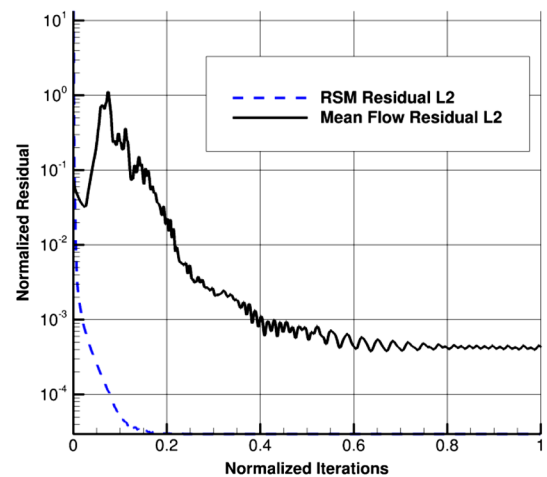


b) DPW-W1 normalized residuals

Fig. 15 Representative convergence information for DPW-W1.



a) DLR-F11 lift and drag coefficients



b) DLR-F11 normalized residuals

Fig. 16 Representative convergence information for DLR-F11 (high Re , no brackets), $\alpha = 7$ deg.

of 10^{-3} and 10^{-4} , respectively. It should also be noted that for the DLR-F11 configuration, FUN3D had to be run past the point of the lift and drag coefficients reaching a steady value to obtain a converged solution for the velocity profiles, and it was typical to run FUN3D for greater than 20,000 iterations to achieve convergence.

VI. Conclusions

Overall this study of the stress- ω RSM was conducted to further assess its ability to accurately simulate external flow over wings. The NASA Langley FUN3D and CFL3D codes were both used to simulate flow over the high-lift DLR-F11 configuration, with the focus of this paper being primarily on the FUN3D results. The DPW-W1 was representative of a wing-alone case in a cruise configuration, and was intended to show that RSM could give results consistent with results from different codes run on a consistent grid. The wing surface pressures predicted by the RSM were nearly identical to those predicted by FUN3D and CFL3D using the SA turbulence model, and the skin friction coefficients less consistent, but still very similar, showing that the RSM is less dissipative than the SA model, as expected. This consistency is encouraging, as it helps validate the implementation of the RSM in FUN3D, and further study would benefit from experimental measurements of the DPW-W1 wing configuration to assess the accuracy of these models in predicting the pressure and skin friction coefficients.

For the DLR-F11 wing-body high-lift configuration, the RSM results were largely encouraging. Overall, the RSM performed better than the one-equation Spalart-Allmaras turbulence model at the 18.5 angle of attack case in many predictions, but showed results comparable to the two-equation SST-V turbulence model. This is consistent with the results seen running the RSM on NASA Trapezoidal Wing in the previous study [1]. The RSM predictions of C_p did better match the experimental measurements at an 18.5 deg angle of attack than the SA turbulence model, especially on the outboard flap. Also, the drag predicted by the RSM was much closer to the measured value at higher angles of attack than the SA or SST-V turbulence models, but there were large discrepancies in results between the models, suggesting underlying grid resolution issues. The performance of both models was very poor overall in capturing the velocity profile measured in the B-LSWT; however, the RSM did do better in regions where the wake has influence, on the outboard flap.

It is also encouraging that both CFL3D and FUN3D are able to obtain a converged RSM solution for a complex wing geometry that was largely similar. Since the RSM results clearly showed improvements over the SA turbulence model and performed comparably to the SST-V model, there is the cost-benefit question of whether the RSM is worth the extra computation. We believe that it is. The the 2006 Wilcox Stress- ω model is shown here to be a robust turbulence model, and should be further studied to better assess its

merits. Future studies leave open the possibility of collecting skin friction experimental data and comparing the RSM to other two-equation turbulence models to assess whether other models perform as well in the outboard flap of the DLR-F11 configuration, where the RSM seems to be most accurate.

Acknowledgments

The research is supported in part by NASA Cooperative Agreement NNX11AI56A, funded under the Aeronautical Sciences Project of the Fundamental Aeronautics Program. Chris Rumsey is the Technical Monitor. The authors would like to thank Chris Rumsey and Elizabeth Lee-Rausch of NASA Langley for their support with FUN3D and CFL3D, and providing additional results from the 2nd High Lift Prediction Workshop.

References

- [1] Rodio, J. J., Xiao, X., Hassan, H. A., and Rumsey, C. L., "NASA Trapezoidal Wing Simulation Using Stress- and One- and Two-Equation Turbulence Models," *52nd Aerospace Sciences Meeting*, AIAA Paper 2014-0404, 2014.
- [2] Krist, S. L., Biedron, R. T., and Rumsey, C. L., "CFL3D User's Manual (Ver. 5.0)," NASA TM-1998-208444, June 1998.
- [3] Wilcox, D. C., *Turbulence Modeling for CFD*, 3rd ed., DCW Industries, LA Canada, CA, 2006, pp. 332–334.
- [4] Eisfeld, B., "Differential Reynolds Stress Modeling at DLR Status & Perspectives," presentation, NASA Langley Research Center, Hampton, VA, April 2014.
- [5] Biedron, R. T., Derlaga, J. M., Gnoffo, P. A., Hammond, D. P., Jones, W. T., Kleb, B., Lee-Rausch, E. M., Nielsen, E. J., Park, M. A., Rumsey, C. L., Thomas, J. L., and Wood, W. A., NASA TM-2014-218520, March 2014.
- [6] Lee-Rausch, E. M., Rumsey, C. L., and Hammond, D. P., "FUN3D Analysis of DPW-III Wing/Body Configurations," presentation, *3rd AIAA Drag Prediction Workshop*, San Francisco, CA, June 2006.
- [7] Rumsey, C. L., and Slotnick, J. P., *Overview and Summary of the Second AIAA High Lift Prediction Workshop (Invited)*, AIAA Paper 2014-0747, 2014.
- [8] Spalart, P. R., and Allmaras, S. R., "A One-Equation Turbulence Model for Aerodynamic Flows," *Recherche Aerospaciale*, No. 1, 1994, pp. 5–21.
- [9] Roe, P. L., "Approximate Riemann Solvers, Parameter Vectors, and Difference Schemes," *Journal of Computational Physics*, Vol. 43, No. 2, 1981, pp. 357–372.
- [10] Burg, C. O. E., Sheng, C., Newman, J. C., III, Brewer, W., Blades, E., and Marcum, D. L., "Verification and Validation of Forces Generated by an Unstructured Flow Solver," AIAA Paper 2003-3983, 2003.
- [11] Eisenstat, S. C., Elman, H. C., and Schultz, M. H., *SIAM Journal on Numerical Analysis*, Vol. 20, No. 2, April 1983, pp. 345–357. doi:10.1137/0720023
- [12] Menter, F. R., "Two-Equation Eddy-Viscosity Turbulence Models for Engineering Applications," *AIAA Journal*, Vol. 32, No. 8, 1994, pp. 1598–1605. doi:10.2514/3.12149
- [13] Eliasson, P., "Investigation of a Half-Model High-Lift Configuration in a Wind Tunnel," *Journal of Aircraft*, Vol. 45, No. 1, 2008, pp. 29–37. doi:10.2514/1.34054.